Article

Micromechanical Simulation of Thermal Cyclic Behavior of ZrO$_2$/Ti Functionally Graded Thermal Barrier Coatings

Hideaki Tsukamoto

Graduate School of Engineering, Nagoya Institute of Technology, Gokiso-cho, Showa-ku, Nagoya, Aichi, 466-8555, Japan; E-Mail: tsukamoto.hideaki@nitech.ac.jp; Tel./Fax: +81-52-735-7914

Abstract: This study numerically investigates cyclic thermal shock behavior of ZrO$_2$/Ti functionally graded thermal barrier coatings (FG TBCs) based on a nonlinear mean-field micromechanical approach, which takes into account the time-independent and dependent inelastic deformation, such as plasticity of metals, creep of metals and ceramics, and diffusional mass flow at the ceramic/metal interface. The fabrication processes for the FG TBCs have been also considered in the simulation. The effect of creep and compositional gradation patterns on micro-stress states in the FG TBCs during thermal cycling has been examined in terms of the amplitudes, ratios, maximum and mean values of thermal stresses. The compositional gradation patterns highly affect thermal stress states in case of high creep rates of ZrO$_2$. In comparison with experimental data, maximum thermal stresses, amplitudes and ratios of thermal stresses can be effective parameters for design of such FG TBCs subject to cyclic thermal shock loadings.

Keywords: functionally graded thermal barrier coatings (FG TBCs); thermal cycle; micromechanics; creep; compositional gradation

1. Introduction

Ceramic-metal functionally graded thermal barrier coatings (FG TBCs) have been attracting a great deal of attention for structures working under super high temperatures and temperature gradients. A unique blend of material properties make them good candidates for the use in various structural components demanding high strength, high resistance to heat, and low weight, which is of particular interest in the modern transportation and aerospace industries [1,2].

FG TBCs are advanced multiphase composites that are engineered to have a smooth spatial variation of material constituents. This variation results in an inhomogeneous structure with smoothly varying thermal and mechanical properties. The advantages of FG TBCs as an alternative to two dissimilar materials (ceramics and metal) joined directly together include smoothing of thermal stress distributions across the layers, minimization or elimination of stress concentrations and singularities at the interface corners and increase in bonding strength [3].

FG TBCs are macroscopically and microscopically heterogeneous. Macroscopic heterogeneity means the gradation of microstructures and material properties through the thicknesses of the FG TBCs, and microscopic heterogeneity is due to the fact that the composite materials are composed of several constituents, usually metals and ceramics. In order to make the best use of such heterogeneous materials, the formulation of the constitutive relation from the standpoints of these two different scales is required [4,5].

So far a number of analytical and computational methods to predict thermal stress states in functionally graded materials (FGMs) and design optimal FGMs have been proposed [6,7]. Some of them considered macroscopic heterogeneity, and used the simple rules of mixture such as Voghit and Reuss rules to derive effective properties of the composites. Some studies take into more account the microscopic heterogeneity. These studies are classified into two categories. One adopts finite element methods, which assume periodic microstructure of compositions in FGMs [8,9]. The other is an analysis based on micromechanics, one of which is the Eshelby's equivalent inclusion method [10–12] being effective and applicable to analyze high-temperature behavior of ceramic-metal composites. An earlier work by Wakashima and Tsukamoto [13,14] applied the mean-field micromechanical concepts to estimating the thermal stresses in a FGM plate. Up to date, many studies have been done based on such micromechanical concepts [15,16].

From the viewpoints of what kinds of inelastic deformations for each phase to be taken into account, some studies [17] considered plastic deformation of metal phase, which is the time-independent deformation, and some studies [18] took into consideration time-dependent deformation such as creep in FG TBC plates, for which the constitutive relations derived from experimental results were used. Recently, micromechanical approach considering plastic deformation of metal phase and creep of metal and ceramic phase as well as diffusional mass flow at the interface between metal and ceramic phases is proposed by the author [5].

In the past decade, ZrO_2/Ti FG TBCs have been of potential for high-temperature applications in automobile and aerospace industries. ZrO_2 has superior thermal and mechanical properties, which are effective for TBCs [19]. One of superior mechanical properties of ZrO_2 is high fracture toughness due to stress-induced transformation (from tetragonal to monoclinic crystal structures under some stress conditions, which can be used in enhancement of fracture toughness of various ceramics and ceramic matrix composites [20–22].

The purpose of the current study is to numerically investigate thermal cyclic behavior of ZrO_2/Ti functionally graded thermal barrier coatings (FG TBCs) based on a nonlinear mean-field micromechanical approach [5], which takes into account the time-independent and dependent inelastic deformation, such as plasticity of metals, creep of metals and ceramics, and diffusional mass flow at the ceramic/metal interface. The fabrication processes for the FG TBCs have been also considered. The effect of compositional gradation patterns and time-dependent inelastic deformation on micro-stress states in the

FG TBCs during thermal cycling has been examined in terms of the amplitudes, ratios and mean values of thermal stresses.

2. Mean-Field Micromechanics-Based Analysis

2.1. Basic Model

The model used in the study is based on the work by Tsukamoto [5]. A brief description of the model is made here. Macroscopically homogeneous composites with spherical particles are considered to be building blocks of the functionally graded thermal barrier coating (FG TBC) plate as shown in Figure 1. The building blocks are assumed to be subject to balanced bi-axial plane stresses. Here, the metal phase is assumed to be matrix and ceramic phase is particles, which are indicated by subscript 0 and 1, respectively, while the inversion of the relation of matrix and particles can be easily derived in the similar way. The inelastic deformation of constituents of the composites include creep with the strain, ε^c, plastic deformation with the strain, ε^p, and diffusional mass transport along the metal-ceramic interface with the eigen strain of the particle, ε^d. The in-plane and out-of-plane micro-stresses in each phase can be written as follows [5],

$$\sigma_0^{in} = 2(\beta_0 + 1/3\gamma_0)\sigma + 3f_1\beta^*(\alpha_1 - \alpha_0)\theta + 2f_1\gamma^*\left\{(\varepsilon_1^c - \varepsilon_0^c) + \varepsilon^d - \varepsilon^p\right\} \tag{1}$$

$$\sigma_0^{out} = 2(\beta_0 - 2/3\gamma_0)\sigma + 3f_1\beta^*(\alpha_1 - \alpha_0)\theta - 4f_1\gamma^*\left\{(\varepsilon_1^c - \varepsilon_0^c) + \varepsilon^d - \varepsilon^p\right\} \tag{2}$$

for the metal matrix (indicated by subscript 0), and

$$\sigma_1^{in} = 2(\beta_1 + 1/3\gamma_1)\sigma - 3f_0\beta^*(\alpha_1 - \alpha_0)\theta - 2f_0\gamma^*\left\{(\varepsilon_1^c - \varepsilon_0^c) + \varepsilon^d - \varepsilon^p\right\} \tag{3}$$

$$\sigma_1^{out} = 2(\beta_1 - 2/3\gamma_1)\sigma - 3f_0\beta^*(\alpha_1 - \alpha_0)\theta + 4f_0\gamma^*\left\{(\varepsilon_1^c - \varepsilon_0^c) + \varepsilon^d - \varepsilon^p\right\} \tag{4}$$

for the ceramic particle (indicated by subscript 1).

Here, f_0 and f_1 are the volume fraction, α_0 and α_1 are the coefficient of thermal expansion, and σ is a macro-stress due to balanced bi-axial loadings. β_0, β_1, γ_0, γ_1, β^* and γ^* are micromechanical constants depending on the elastic constants and volume fraction of each phase, which were given in the work by Tsukamoto [5]. The equivalent micro-stresses in each phase are expressed by,

$$\sigma_0^{eq} = \left|\sigma_0^{in} - \sigma_0^{out}\right| = 2\left|\gamma_0\sigma + 3f_1\gamma^*\left\{(\varepsilon_1^c - \varepsilon_0^c) + \varepsilon^d - \varepsilon_0^p\right\}\right| \tag{5}$$

$$\sigma_1^{eq} = \left|\sigma_1^{in} - \sigma_1^{out}\right| = 2\left|\gamma_1\sigma - 3f_0\gamma^*\left\{(\varepsilon_1^c - \varepsilon_0^c) + \varepsilon^d - \varepsilon_0^p\right\}\right| \tag{6}$$

In this analysis, plastic and creep deformations are supposed to obey the associated flow rule in which both deformation potentials are taken equal to the von Mises-type yield function. Plastic deformation of metal phase is assumed to be expressed by the Swift's equation:

$$\sigma_0^{eq} = a(c + \varepsilon^{p\,eq})^{n_p} \tag{7}$$

where a, c and n_p are constants. σ_0^{eq} is the (equivalent) flow stress of metals. When the creep deformation of each phase is assumed to be controlled by grain-boundary diffusion (Coble creep), the constitutive equation is expressed as follows,

$$\dot{\varepsilon}_{\text{coble}}^{\text{c}}{}^{\text{eq}} = C\frac{\omega_{\text{gb}}D_{\text{gb}}\Omega}{kTd^3}\sigma^{\text{eq}} \tag{8}$$

C is the geometric constant (~16), D_{gb} the grain boundary diffusivity, ω_{gb} the grain boundary width, Ω the volume of a diffusing atom, d the grain size and k the Boltsman's constant. The inelastic strain $\dot{\varepsilon}^{\text{d}\,\text{eq}}$ by mass transport along the interface between metal and ceramic phases is expressed as follows [5],

$$\dot{\varepsilon}^{\text{d}\,\text{eq}} = C^{\text{int}}\frac{\omega_{\text{int}}D_{\text{int}}\Omega}{kTd_{\text{p}}^3}\sigma_1^{\text{eq}} \tag{9}$$

C^{int} is the material constant derived from micromechanical considerations, ω_{int} the interface width for diffusion, D_{int} the interfacial diffusivity, Ω the volume of diffusing atom and d_{p} the diameter of the particle. Therefore, when considering the composites under plane-stress conditions, the constitutive equations can be described by

$$\dot{\sigma}(z,t) = \left\{S^{\text{e}}(z) + S^{\text{p}}(z,t)\right\}\left\{\dot{\varepsilon}(z,t) - \alpha(z)\dot{\theta}(z,t) - \dot{\varepsilon}^{\text{p(cd)}}(z,t) - \dot{\varepsilon}^{\text{c-d}}(z,t)\right\} \tag{10}$$

$\dot{\sigma}(z,t)$ is the plane stress rate, $S^{\text{e}}(z)$ the overall plane-stress elastic compliance, $S^{\text{p}}(z,t)$ the overall plane-stress plastic compliance, $\alpha(z)$ the overall in-plane thermal expansion coefficient, $\dot{\varepsilon}^{\text{p(cd)}}(z,t)$ the overall plastic strain rate due to the difference between creep abilities of each phase and interfacial diffusion, and $\dot{\varepsilon}^{\text{c-d}}(z,t)$ the overall creep strain rate. The details for mathematical expressions of these functions are given in the work by Tsukamoto [5]. $\dot{\sigma}(z,t)$ given in Equation (10) can be incorporated with the lamination theory.
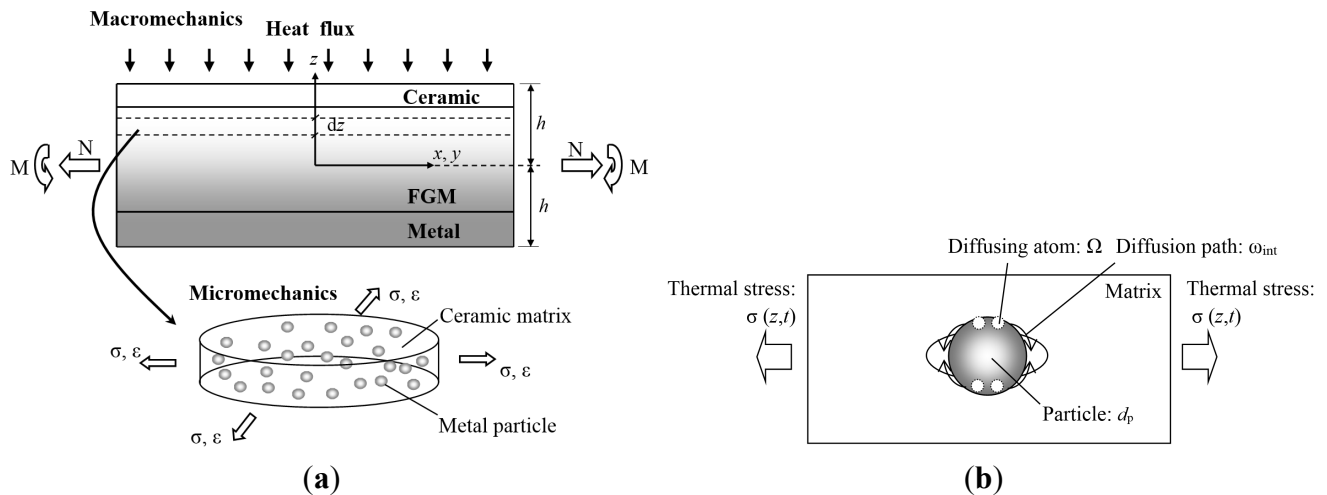

Figure 1. Schematic illustration of (**a**) a functionally graded thermal barrier coatings (FG TBCs) subjected to thermo-mechanical loadings and its building block of the thin layer composed of spherical particle-dispersed composites, and (**b**) mass transfer at the particle/matrix interface.

2.2. Simulation Input Data

Now let us consider cyclic thermal behavior of ZrO_2/Ti FG TBCs to be analyzed. The FG TBCs have a thickness of 9 mm, in which the FGM part has a thickness of 3 mm and Ti substrate part has that of 6 mm. The FGM part (3 mm) consists of six composite layers with different compositions according to

predetermined compositional gradation patterns of the FGMs. Figure 2 shows the compositional gradation patterns used in this study. Step-wised compositional gradation patterns are parametrically described using the following expression [4,5].

$$f_m(i) = 1 - f_c(i) = (i-1)^n / (P-1)^n \qquad (11)$$

where, $f_m(i)$ and $f_c(i)$ are the volume fractions of metal (Ti) and ceramics (ZrO$_2$) phases in the i-th sub-layer, respectively. P is the total number of sub-layers, which have the thickness of 0.5 mm for each in the FGM part. The exponent, n, is a parameter characterizing the compositional gradation pattern. For the gradation parameter n, $n = 1$ means the linear compositional gradation, $n > 1$ means the ceramic-rich gradation and $n < 1$ means the metal-rich gradation. In this study, FGM samples with three different compositional gradation patterns of $n = 0.5$, 1 and 2 were simulated to investigate the effects of compositional gradation patterns on the thermo-mechanical behavior.
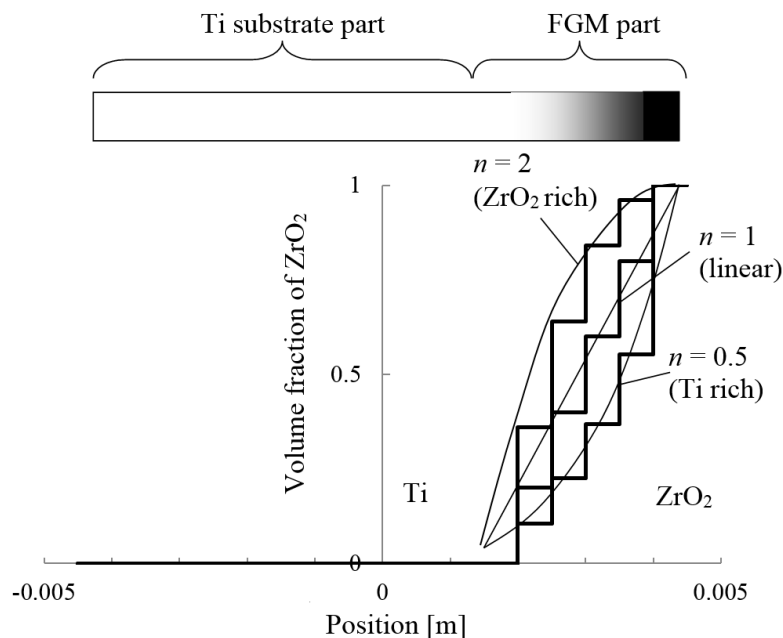

Figure 2. Compositional gradation patterns of FG TBCs.

The material property data of Ti and ZrO$_2$ used in the calculations are shown in Table 1. The total thickness of the samples is set at 9 mm (including 3 mm thickness for the FGM part and 6 mm thickness for the substrate part). The thermo-mechanical boundary conditions considered here are illustrated in Figure 3, and described as follows. The powders to be sintered is stuffed in dice (fully constraint in both in-plane and out-of-plane deformations) at 1400 °C. Under this condition, there is no stress in the samples. Then temperature of samples goes down to room temperature (R.T.) at the cooling rate of 100 °C/min under the mechanical boundary conditions of fully constraint deformation. At R.T., all the mechanical constraints are relieved (free mechanical constraint). After that, cyclic thermal shock tests start. The ceramic surface is assumed to be heated to 1200 °C for 1 min. After the temperature of the ceramic surface reaches 1200 °C, the temperature is hold for 60 s. Then the ceramic surface is exposed to the air with the heat transfer coefficient of 300 W/(m^2 K) and temperature of R.T. during cooling processes. The air-cooling processes take 60 s, and then the ceramic surface is suddenly cooled down to

R.T. During cyclic thermal shock tests Ti substrate sides are exposed to air with the heat transfer coefficient of 500 W/(m^2 K) all the time. This process corresponds to one cycle, which is repeated 4 times in the simulation like the current experiments. Based on the micromechanical model, the program codes for analysis of thermo-mechanical behavior of FGMs were developed using Fortran 95 programming languages. The simulation was conducted on laptop computer with normal specifications.

Table 1. Material property data of Ti and ZrO$_2$ used in the calculation. Diameter of a particle is 40×10^{-6} m, $D_{int} \times \omega_{int}$ is assumed to be the same value as $D_{gb} \times \omega_{gb}$ for Ti. Flow stress parameters in Swift equation for Ti are $a = 600$ MPa, $c = 0.3$ and $n = 1$.

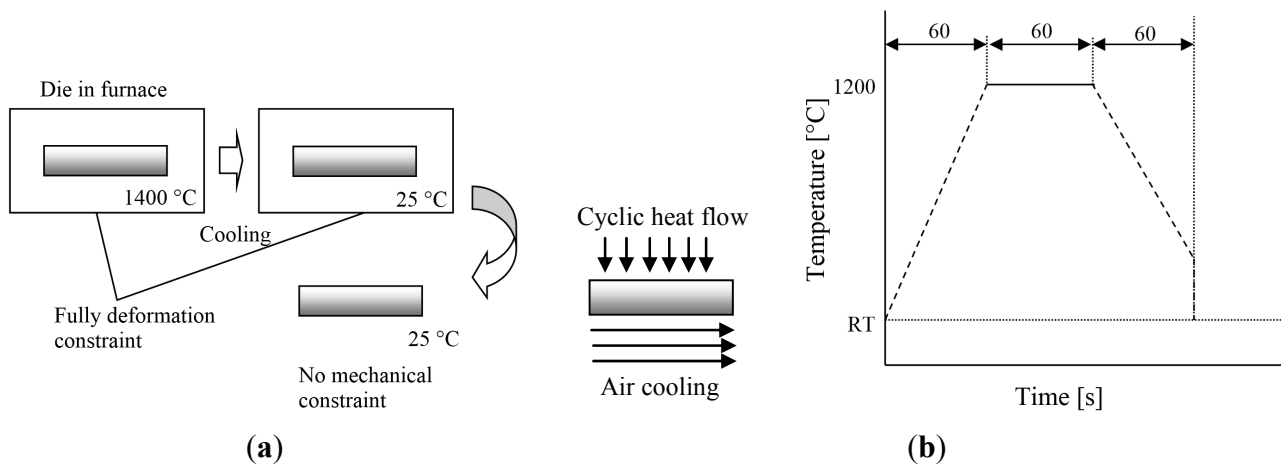| Property data	Ti	ZrO$_2$
Young's moduluns [GPa]	116	200
Poisson's ration	0.32	0.3
CTE 10^{-6} [K^{-1}]	8.6	10.0
Thermal conductivity [Wm^{-1} K^{-1}]	21.9	3.0
Specific heat [J kg^{-1} K^{-1}]	520	3000
Density[kg m^{-3}]	4506	5990
Coble creep parameters		
D_{gb0}(pre-exp. Term) $\times \omega_{gb}$ [m^{-3} s^{-1}]	1.9×10^{-7}	0.29×10^{-6}
Activation energy [J mol^{-1}]	1.53×10^{5}	5.7×10^{5}
Atomic volume [m^3]	1.15×10^{-29}	4.66×10^{-29}
Grain size[m]	10.0×10^{-6}	0.1, 1 and 10.0×10^{-6}

(a) **(b)**

Figure 3. Schematic illustration of thermo-mechanical boundary conditions for fabrication and thermal cycling processes: (**a**) fabrication process, and (**b**) thermal cycling process, including a schematic illustration of heat flow and temperature profile for one cycle.

2.3. Simulation Results

Figure 4 shows calculation results of temperature transient of the ZrO$_2$ surface and maximum stress transient in the ZrO$_2$ surface layer during fabrication and cyclic thermal shock test processes. It is seen in Figure 4a,b that maximum stresses in the ZrO$_2$ surface layer vary with temperature transients. The highest stresses can be reached just after the fabrication (at point A in Figure 4a,b). During cyclic thermal shock tests, the maximum stresses in the ZrO$_2$ surface layer change with temperature transients, in which

high maximum stress peaks are reached at R.T. Now let us define three parameters such as the mean stress, σ_{mean}, range, $\Delta\sigma$, and ratio, R, of the maximum thermal stresses. To begin with, it is set σ_{max} the high peak value of maximum thermal stresses in the ZrO_2 surface layer at R.T. in a cycle, and σ_{min} the low peak value of the maximum thermal stresses in the ZrO_2 surface layer at 1200 °C in a cycle. The mean stress, σ_{mean}, is defined by $(\sigma_{max} + \sigma_{min})/2$. The range of stress, $\Delta\sigma$, is defined by $\sigma_{max} - \sigma_{min}$. The ratio of stress, R, is defined by $\sigma_{min}/\sigma_{max}$.
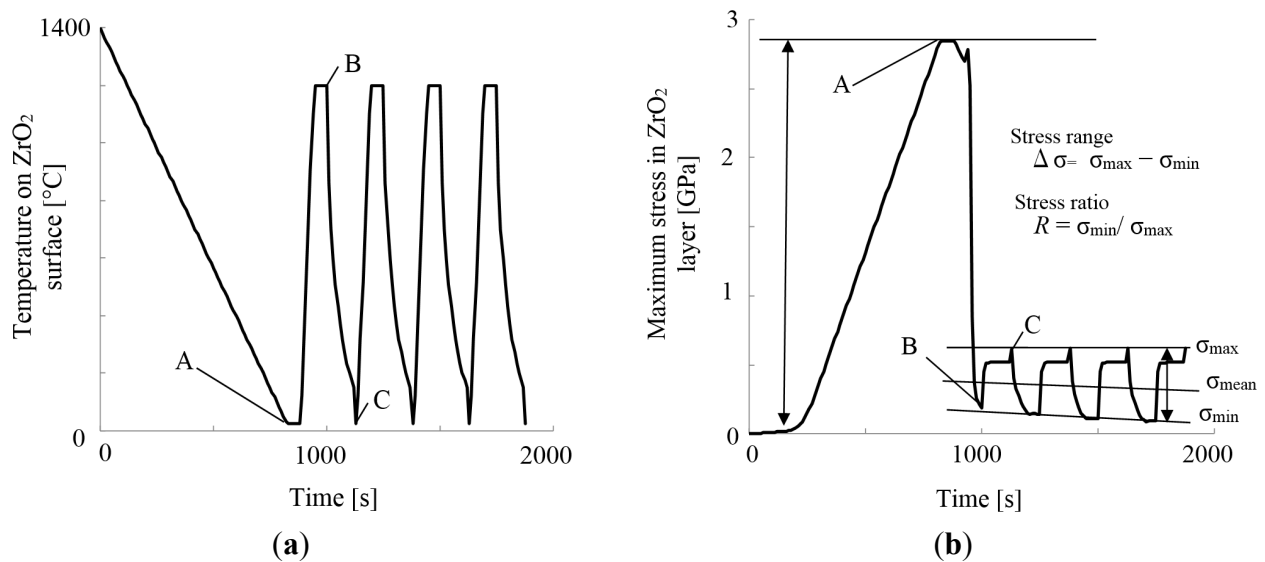

Figure 4. Temperature transient of ZrO_2 surface (**a**) and maximum thermal stress transient in ZrO_2 surface layer (**b**) during fabrication and cyclic thermal shock processes. Points A, B and C shown in the figures indicates the corresponding points, at which the time is the same.

Residual stress states in the ZrO_2 surface layer just after the fabrication process are shown in Figure 5, which includes the effect of creep ability (grain size) of ZrO_2 and compositional gradation patterns on the residual stress states. It is seen that there is almost no difference among the FG TBCs with different compositional gradation patterns, while creep rates represented by grain sizes (0.01, 1 and 10 µm) of ZrO_2 (corresponding to creep ability expressed by Equation 8) highly affect the residual stress states. In any cases, maximum residual stresses in ZrO_2 layers are tensile. In case of the grain size of ZrO_2 of 0.01 µm, corresponding to high creep rates maximum residual stresses are low compared to others, which is attributed to high creep rates of ZrO_2 leading to large creep deformation during the cooling process in the fabrication.

Figure 6 shows the maximum thermal stresses, σ_{max}, and mean thermal stresses, σ_{mean}, in ZrO_2 surface layer during cyclic thermal shock loading tests in case of $d_{ZrO_2} = 0.01$ µm and $d_{ZrO_2} = 10$ µm. The effect of creep of ZrO_2 can be apparently seen in the figures. For σ_{max}, the order for composition gradation patterns is different between $d_{ZrO_2} = 0.01$ µm and $d_{ZrO_2} = 10$ µm. In case that the creep rates of ZrO_2 is high ($d_{ZrO_2} = 0.01$ µm), FG TBCs with $n = 2$ shows higher σ_{max} than others, while FG TBCs with $n = 0.5$ shows higher σ_{mean} than others. Meanwhile, in case that creep rates of ZrO_2 is low ($d_{ZrO_2} = 10$ µm), FG TBCs with $n = 0.5$ shows higher σ_{max} than others, and FG TBCs with $n = 0.5$ also shows higher σ_{mean} than others.
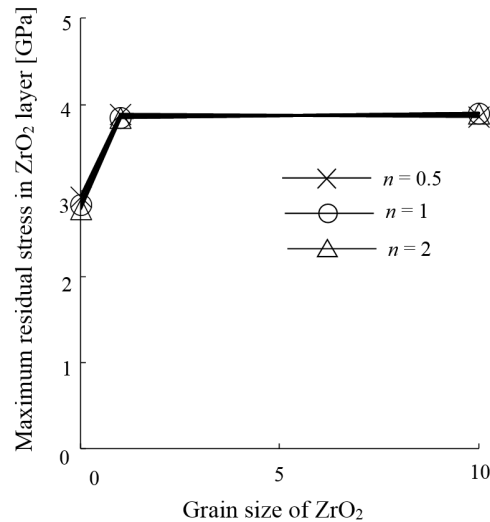
Figure 5. Residual stress states in the ZrO_2 surface layer just after fabrication processes for functionally graded materials (FGMs) with $n = 0.5$, 1 and 2.
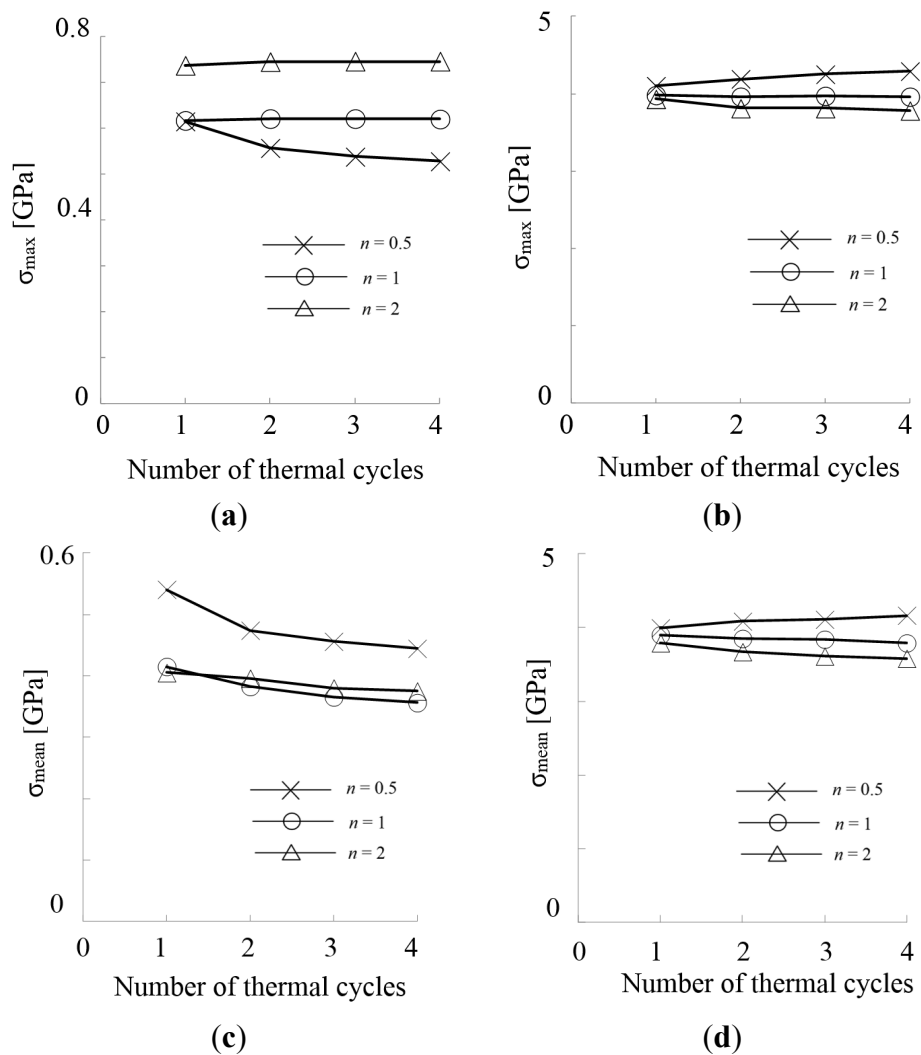

Figure 6. Maximum thermal stresses, σ_{max}, and mean thermal stresses, σ_{mean}, in ZrO_2 surface layer during thermal shock cycling. (**a**) σ_{max} for $d_{ZrO_2} = 0.01$ μm, (**b**) σ_{max} for $d_{ZrO_2} = 10$ μm, (**c**) σ_{mean} for $d_{ZrO_2} = 0.01$ μm, and (**d**) σ_{mean} for $d_{ZrO_2} = 10$ μm.

Figure 7 shows the amplitudes (ranges), $\Delta\sigma$, and ratios, R, of thermal stresses in the ZrO_2 surface layer during cyclic thermal shock loading tests for $d_{ZrO_2} = 0.01$ μm and for $d_{ZrO_2} = 10$ μm. Creep of ZrO_2 largely affects $\Delta\sigma$ and R. For $\Delta\sigma$, in case of both low and high creep rates of ZrO_2, FG TBCs with $n = 2$ shows higher $\Delta\sigma$ than others. It is expected that when the thermal fatigue behavior is dominant, FG TBCs with $n = 2$ exhibit the lowest resistance to such cyclic thermal shock loadings. For R, in case of low creep rates of ZrO_2 ($d_{ZrO_2} = 10$ μm), FG TBCs with any compositional gradation patterns show almost the same and constant values, which are not also affected by number of thermal cycles.
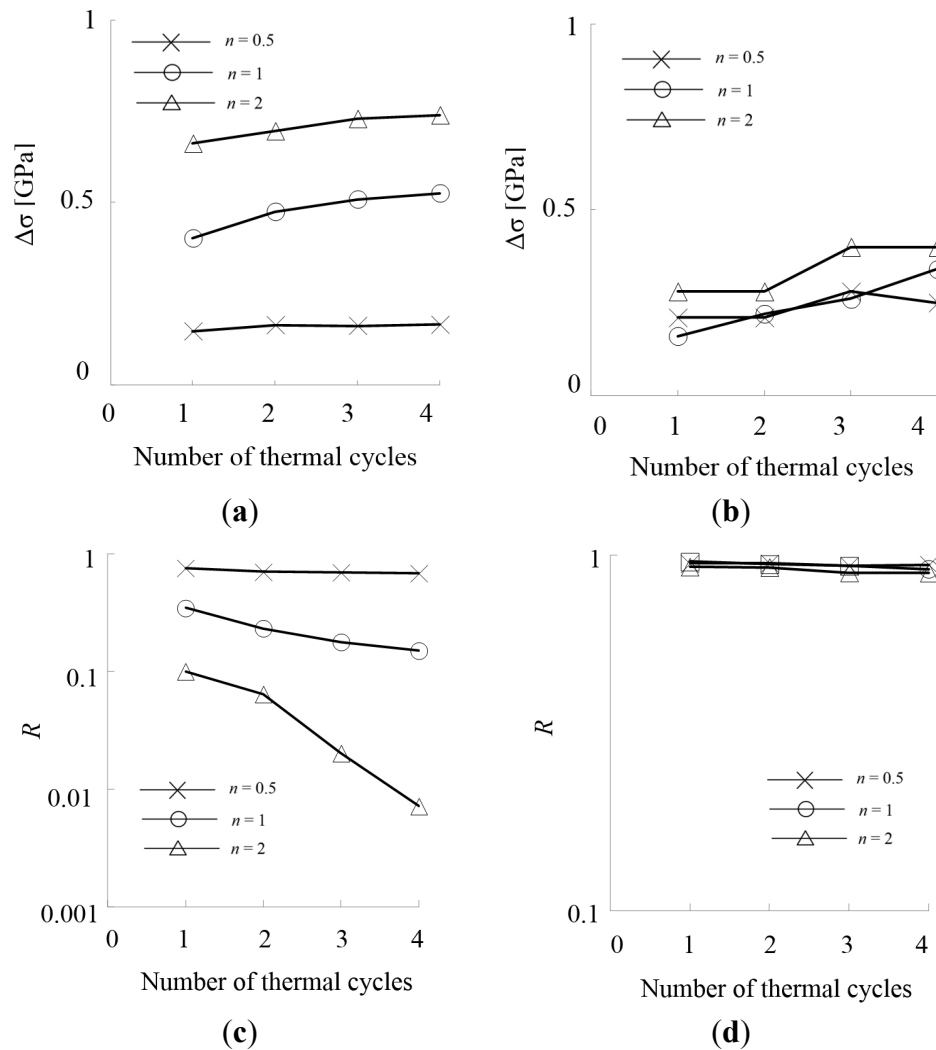

Figure 7. Amplitudes, $\Delta\sigma$, and ratios, R, of thermal stresses in ZrO_2 surface layer during thermal shock cycling. (**a**) $\Delta\sigma$ for $d_{ZrO_2} = 0.01$ μm, (**b**) $\Delta\sigma$ for $d_{ZrO_2} = 10$ μm, (**c**) R for $d_{ZrO_2} = 0.01$ μm, and (**d**) R for $d_{ZrO_2} = 10$ μm.

Maximum equivalent thermal stresses, σ_{max}^{eq}, in ZrO_2 surface layer during cyclic thermal shock loading tests for $d_{ZrO_2} = 0.01$ μm and for $d_{ZrO_2} = 10$ μm are shown in Figure 8. It is seen that in case of high creep rates of ZrO_2 ($d_{ZrO2} = 0.01$ μm), FG TBCs with $n = 2$ shows higher σ_{max}^{eq} than others, while in case of low creep rates of ZrO_2 ($d_{ZrO_2} = 10$ μm), FG TBCs with $n = 0.5$ shows higher σ_{max}^{eq} than others. This tendency is the same as that of σ_{max}.
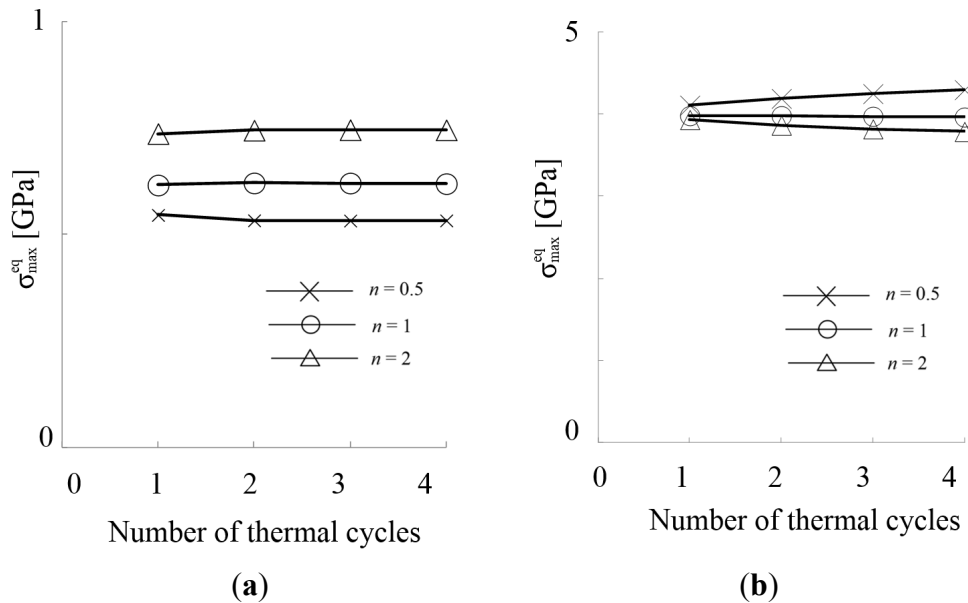
Figure 8. Maximum equivalent thermal stresses, σ_{max}^{eq}, in ZrO_2 surface layer during thermal shock cycling. (**a**) σ_{max}^{eq} for $d_{ZrO_2} = 0.01$ μm; (**b**) σ_{max}^{eq} for $d_{ZrO_2} = 10$ μm.

Amplitudes (ranges) of thermal stresses, $\Delta\sigma$, plotted against mean stresses, σ_{mean} are shown in Figure 9. The data can be classified into two regimes. It can be seen that in case of high creep rates of ZrO_2 ($d_{ZrO_2} = 0.01$ μm), the values of σ_{mean} are very low compared to values for low creep rates of ZrO_2 ($d_{ZrO_2} = 1$ and 10 μm).
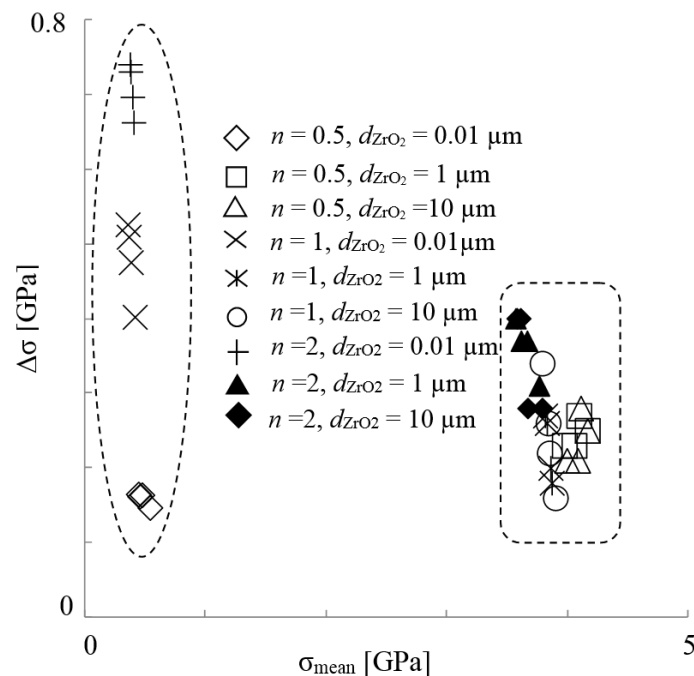
Figure 9. Amplitudes of thermal stresses, $\Delta\sigma$ plotted against mean stress, σ_{mean}.

$\Delta\sigma$ scatters over the wide ranges highly depending on compositional gradation patterns, n, in case of high creep rates of ZrO_2, in which higher value of n leads to higher $\Delta\sigma$. $\Delta\sigma - \sigma_{mean}$ graph is in general used for examining the fatigue limits. σ_{mean} value is high compared to $\Delta\sigma$ value in case of low creep rates

of ZrO_2, while σ_{mean} and $\Delta\sigma$ values are similar and small in case of high creep rates of ZrO_2. These results are considered to be due to creep of ZrO_2 in cooling processes under cyclic thermal shock conditions.

3. Experimental Data

Now let us examine the simulation results including extracted micromechanical parameters shown above based on experimental data. Here, consider the FGM samples, which were fabricated using spark plasma sintering (SPS) methods [23]. The ingredient powders were ZrO_2 partially-stabilized by 3 mol% Y_2O_3. The average diameter of ZrO_2 powder is 26 nm, and that of Ti powder is less than 45 μm. The SPS was conducted in vacuum at 1400 °C under the uniaxial pressure of 30 MPa with the time duration of 20 min. The sintered FGM samples have a diameter of 20 mm and the same total and layer thicknesses as input data used in the simulation. The compositional gradation patterns of the FGMs are also the same as used in the calculations, that is, $n = 0.5$, 1 and 2. For thermal cycling, the profile of temperature of the ZrO_2 surface used in the experiments is the same as used in the simulation and shown in Figure 3, except for the cooling process. In the experiment, cooling was performed for the time duration of 1800 s, in which the temperature of ZrO_2 surface turned to R.T. (around 25 °C).

Figure 10 shows the relation between the total length of cracks in ZrO_2 surface layer of the FG TBC samples and number of thermal shock cycles. It can be seen in Figure 10 that the total length of cracks increases with increasing number of thermal shock cycles. The FGMs with higher ZrO_2 content, which corresponds to higher value of n, show higher total length of cracks generated on ZrO_2 surfaces and are easier to fracture in the FGMs under such cyclic thermal shock loading conditions. Among the tested samples, FGMs with $n = 0.5$ show the highest resistance to cyclic thermal shock loadings.
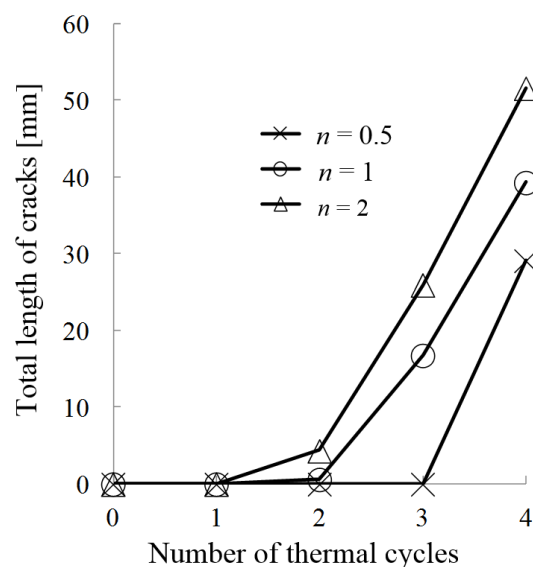
Figure 10. Cyclic thermal shock fracture behavior of FG TBCs. Relation between total length of cracks on ZrO_2 surface and number of thermal cycles is shown.

In the experiment, the average diameter of ZrO_2 powder is 26 nm, so it is reasonable to refer to simulation results for $d_{ZrO_2} = 0.01$ μm (10 nm). As to thermal fatigue behavior, it is considered with simulation results shown in Figure 6c that mean stresses, σ_{mean}, do not so much affect the cyclic thermal

shock fracture behavior of the FG TBCs because even if σ_{mean} is high, resistance to cyclic thermal shock loadings is high for $n = 0.5$. Meanwhile, it is seen in Figure 6a that higher n corresponds to higher σ_{max}, which is reasonable to explain experimental results on cyclic thermal shock fracture behavior of the FG TBCs. It is also seen in Figure 7a that higher *n* corresponds to higher $\Delta\sigma$, which is reasonable to explain experimental results, in which higher n leads lower resistance to thermal shock loadings. For the ratio of maximum stress, *R*, it is seen in Figure 7c that higher n corresponds to lower *R*, which is also reasonable in connection with experimental data. With increasing number of thermal cycles, *R* decreases in cases of $n = 1$ and 2, while *R* is almost constant in case of $n = 0.5$. It is seen in Figure 8a that σ_{max}^{eq} is also possibly a reasonable indicator for such fracture. In case of high creep rates of ZrO_2 ($d_{ZrO_2} = 0.01$ μm), FG TBCs with $n = 2$ shows the highest values and FG TBCs with $n = 0.5$ show the lowest values in both σ_{max} and σ_{max}^{eq}. This simulation result is reasonable to understand the current experimental data.

4. Discussion

Creep of ZrO_2 is considered to largely affect the thermal shock fracture behavior of the FGMs. In comparison of simulation results with experimental data, micromechanical parameters, σ_{max}, σ_{max}^{eq}, $\Delta\sigma$ and *R*, are considered to be reasonable parameters for assessing cyclic thermal shock fracture behavior of ZrO_2/Ti FGMs with high creep rate of ZrO_2. According to Figure 9 showing the relation between $\Delta\sigma$ and σ_{mean}, in case of high creep rates of ZrO_2, σ_{mean} is very low compare to that in case of low creep rates of ZrO_2, which is attributed to creep deformation of ZrO_2 at the beginning of cooling processes under thermal shock loading conditions. As seen in Figures 6 and 8, absolute values of σ_{max}, σ_{max}^{eq} and σ_{mean} are largely different between high creep rates and low creep rates of ZrO_2.

Because σ_{max} and σ_{max}^{eq} are considered to affect the cyclic thermal shock fracture behavior of the FGMs, such a difference need to be considered to engineer the FGMs with low creep rate of ZrO_2 subject to cyclic thermal shock loadings. In general, it is considered that in case that σ_{mean} is high, even small value of $\Delta\sigma$ largely affect the fatigue fracture behavior of the FGMs. Consequently the current simulation results are useful and effective to engineer such kinds of FG TBCs subject to cyclic thermal shock loadings. Parameters extracted from the simulation results are effective to use for predicting the cyclic thermal fracture criterion and design of the FG TBCs.

5. Conclusions

This study numerically investigates cyclic thermal shock behavior of ZrO_2/Ti FG TBCs based on a nonlinear mean-field micromechanical approach, and some micromechanical parameters such as amplitudes, ratios, mean and maximum thermal stresses, and equivalent thermal stresses were examined to be used for engineering such FG TBCs. In the simulation, the fabrication processes for the FG TBCs were taken into account. The effect of creep and compositional gradation patterns on these micromechanical parameters, related to micro-stress states in the FG TBCs, were examined. The findings from the study can be summarized as follows.

1. In case of high creep rates of ZrO$_2$ (d_{ZrO_2} = 0.01 μm), ZrO$_2$-rich FG TBCs (n = 2) shows high maximum stresses, σ_{max}, in ZrO$_2$ layers, while Ti-rich FG TBCs (n = 0.5) shows high mean stresses, σ_{mean}. In case of low creep rates of ZrO$_2$ (d_{ZrO_2} = 10 μm), Ti-rich FG TBCs shows high σ_{max} and Ti-rich FG TBCs with n = 0.5 also shows high σ_{mean}.

2. In case of both low and high creep rates of ZrO$_2$, ZrO$_2$-rich FG TBCs shows high amplitude of thermal stresses, $\Delta\sigma$. For thermal stress ratios, R, in case of low creep rates of ZrO$_2$, FG TBCs with any compositional gradation patterns show almost the same and constant for the number of thermal cycles.

3. In case of high creep rates of ZrO$_2$, ZrO$_2$-rich FG TBCs show high maximum equivalent stresses, $\sigma_{\text{max}}^{\text{eq}}$, while in case of low creep rates of ZrO$_2$, Ti-rich FG TBCs shows high $\sigma_{\text{max}}^{\text{eq}}$.

4. In comparison with experimental data, the simulation results are reasonable and effective to engineer such FG TBCs subject to cyclic thermal shock loadings. In experiment, in case of high creep rates of ZrO$_2$ (d_{ZrO_2} = 0.026 μm), Ti-rich FG TBCs exhibit high resistance to cyclic thermal shock loadings compared to linear and ZrO$_2$-rich FG TBCs. Consequently, the parameters of σ_{max}, $\sigma_{\text{max}}^{\text{eq}}$, $\Delta\sigma$ and R are considered to be effective to estimate the thermal cyclic fracture behavior of the FG TBCs in case of high creep rates of ZrO$_2$.

Nomenclature

σ_0^{in}, σ_1^{in}	In-plane micro-stresses
σ_0^{out}, σ_1^{out}	Out-of-plane micro-stresses
σ_0^{eq}, σ_1^{eq}	Equivalent micro-stresses
α_0, α_1	Coefficient of thermal expansion
f_0, f_1	Volume fraction
ε^{c}	Creep strain
ε^{p}	Plastic deformation with the strain
ε^{d}	Eigen strain of the particle due to diffusional mass transport along the metal-ceramic interface
σ	Macro-stress due to balanced bi-axial loadings
β_0, β_1, γ_0, γ_1, β^*, γ^*	Micromechanical constants depending on the elastic constants and volume fraction of each phase
N	In-plane force
M	Bending moment
a, c, n_{p}	Constants in Swift's equation
C	Geometric constant
D_{gb}	Grain boundary diffusivity
ω_{gb}	Grain boundary width
Ω	Volume of a diffusing atom
k	Boltsman's constant
C^{int}	Material constant derived from micromechanical considerations
ω_{int}	Interface width for diffusion

D_{int}	Interfacial diffusivity
$\acute{\sigma}(z,t)$	Plane stress rate
$S^{e}(z)$	Overall plane-stress elastic compliance
$S^{p}(z,t)$	Overall plane-stress plastic compliance
$\alpha(z)$	Overall in-plane thermal expansion coefficient
$\dot{\varepsilon}^{p(cd)}(z,t)$	Overall plastic strain rate due to the difference between creep abilities of each phase and interfacial diffusion
$\dot{\varepsilon}^{c-d}(z,t)$	Overall creep strain rate
$f_{m}(i), f_{c}(i)$	Volume fractions of metal(Ti) and ceramics(ZrO_2) phases in the i-th sub-layer, respectively
P	Total number of sub-layers
n	Parameter characterizing the compositional gradation pattern

Conflicts of Interest

The author declares no conflict of interest.

References

1. Xiong, H.P.; Kawasaki, A.; Kang, Y.S.; Watanabe, R. Experimental study on heat insulation performance of functionally graded metal/ceramic coatings and their fracture behavior at high surface temperatures. *Surf. Coat. Tech.* **2005**, *194*, 203–214.
2. Khor, K.A.; Gu, Y.W. Thermal properties of plasma-sprayed functionally graded thermal barrier coatings. *Thin Solid Films* **2000**, *372*, 104–113.
3. Miyamoto, Y.; Kaysser, W.A.; Rabin, B.H.; Kaeasaki, A.; Ford, R.G. *Functionally Graded Materials: Design, Processing and Applications*; Springer: New York, NY, USA, 1999.
4. Tsukamoto, H. Design against fracture of functionally graded thermal barrier coatings using transformation toughening. *Mater. Sci. Eng. A* **2010**, 527, 3217–3226.
5. Tsukamoto, H. Analytical method of inelastic thermal stresses in a functionally graded material plate by a combination of micro- and macromechanical approaches. *Comps. Part B Eng.* **2003**, *34*, 561–568.
6. Cho, J.R.; Ha, D.Y. Averaging and finite element discretization approaches in the numerical analysis of functionally graded materials. *Mater. Sci. Eng. A.* **2001**, *302*, 187–196.
7. Giannakopoulos, A.E.; Suresh, S.; Finot, M.; Olsson, M. Elastoplastic analysis of thermal cycling: layered materials with compositional gradients. *Acta Metall. Mater.* **1995**, *43*, 1335–1354.
8. Grujicic, M.; Zhang, Y. Determination of effective elastic properties of functionally graded materials using voronoi cell Finite Element Method. *Mater. Sci. Eng. A.* **1998**, *251*, 64–76.
9. Aboudi, J.; Pindera, M.J.; Arnold, S.M. Higher-order theory for functionally graded materials. *Comps. Part B Eng.* **1999**, *30*, 777–832.
10. Eshelby, J.D. The determination of the elastic field of inclusion and related problems. *Proc. R. Soc. Lond. A* **1957**, *241*, 376–396.
11. Eshelby, J.D. The Elastic field outside an ellipsoidal inclusion. *Proc. R. Soc. Lond. A* **1959**, *252*, 561–569.

12. Eshelby, J.D. Elastic inclusions and inhomogeneities. *Prog. Solid Mech.* **1961**, *2*, 89–140.

13. Wakashima, K.; Tsukamoto, H. Micromechanical approach to the thermomechanics of ceramic-metal gradient materials. In Proceedings of the 1st International Symposium on Functionally Gradient Materials, Sendai, Japan, 8–9 October 1990; pp. 19–26.

14. Wakashima, K.; Tsukamoto, H.; Ishizuka, T. Numerical approach to the elasticplastic analysis of thermal stresses in a ceramic-metal bi-material plate with graded microstructure. In *Modelling of Plastic Deformation Its Engineering Applications*, Proceedings of the 13th Risø International Symposium on Materials Science, Risø National Laboratory, Roskilde, Denmark, 7–11 September 1992; pp. 503–510.

15. Taya, M.; Lee, J.K.; Mori, T. Dislocation punching from interfaces in functionally graded materials. *Acta Mater.* **1997**, *45*, 2349–2356.

16. Tohgo, K.; Masunari, A.; Yoshida, M. Two-phase composite model taking into account the matricity of microstructure and its application to functionally graded materials. *Compos Part A Appl. S.* **2006**, 37, 1688–1695.

17. Mao, Y.Q.; Ai, S.G.; Fang, D.N.; Fu, Y.M.; Chen, C.P. Elasto-plastic analysis of micro FGM beam basing on mechanism-based strain gradient plasticity theory. *Comps Struct.* **2013**, *101*, 168–179.

18. Nejad, M.Z.; Kashkoli, M.D. Time-dependent thermo-creep analysis of rotating FGM thick-walled cylindrical pressure vessels under heat flux. *Int. J. Eng. Sci.* **2014**, *82*, 222–237.

19. Lidong, T.; Wenchao, L. Residual stress analysis of Ti-ZrO$_2$ thermal barrier graded materials. *Mater. Design.* **2002**, *23*, 627–632.

20. Gravie, R.C.; Hannink, R.H.; Pascoe, R.T. Ceramic steels. *Nature.* **1975**, *258*, 704–730.

21. Kelly, P.M.; Rose, L.R.F. The martensitic transformationin ceramics—Its role in transformation toughening. *Prog. Mater. Sci.* **2002**, *47*, 463–557.

22. Lin, K.L.; Lin, C.C. Reaction between titanium and zirconia powders during sintering at 1500 °C. *J. Am. Ceram. Soc.* **2007**, *90*, 2220–2225.

23. Tsukamoto, H.; Kunimine, T.; Yamada, M.; Sato, H.; Watanabe, Y. Microstructure and mechanical properties of Ti-ZrO$_2$ composite fabricated by spark plasma sintering. *Key Eng. Mater.* **2012**, *520*, 269–275.